Two-dimensional blue native/SDS-PAGE analysis of whole cell lysate protein complexes of rice in response to salt stress

Article *in* Journal of plant physiology · June 2016

DOI: 10.1016/j.jplph.2016.05.023

CITATIONS
6

READS
187

6 authors, including:

Amenehsadat Hashemi
University of Applied Science and Technology, Sari, Mazandaran, Iran
4 PUBLICATIONS **55** CITATIONS
SEE PROFILE

Javad Gharechahi
Baqiyatallah University of Medical Sciences
35 PUBLICATIONS **476** CITATIONS
SEE PROFILE

Ghorbanali Nematzadeh
Sari Agricultural Sciences and Natural Resources University
160 PUBLICATIONS **768** CITATIONS
SEE PROFILE

Faezeh Shekari
Royan Institute
20 PUBLICATIONS **886** CITATIONS
SEE PROFILE

Journal of Plant Physiology 200 (2016) 90–101

Contents lists available at ScienceDirect

Journal of Plant Physiology

journal homepage: www.elsevier.com/locate/jplph

Two-dimensional blue native/SDS-PAGE analysis of whole cell lysate protein complexes of rice in response to salt stress

Amenehsadat Hashemi[a], Javad Gharechahi[b,*], Ghorbanali Nematzadeh[c], Faezeh Shekari[e], Seyed Abdollah Hosseini[d], Ghasem Hosseini Salekdeh[d,e,*]

[a] University of Applied Science and Technology, Sari, Mazandaran, Iran
[b] Chemical Injuries Research Center, Baqiyatallah University of Medical Sciences, Tehran, Iran
[c] Faculty of Agronomy, University of Agricultural Sciences and Natural Resources of Sari, Sari, Iran
[d] Department of Systems Biology, Agricultural Biotechnology Research Institute of Iran, Agricultural Research, Education, and Extension Organization, Karaj, Iran
[e] Department of Molecular Systems Biology at Cell Science Research Center, Royan Institute for Stem Cell Biology and Technology, ACECR, Tehran, Iran

ARTICLE INFO

Article history:
Received 11 February 2016
Received in revised form 22 May 2016
Accepted 25 May 2016
Available online 22 June 2016

Keywords:
Protein-protein interaction
2D-BN/SDS-PAGE
Complexomics
Protein complexes
Rice
Salt stress

ABSTRACT

To understand the biology of a plant in response to stress, insight into protein-protein interactions, which almost define cell behavior, is thought to be crucial. Here, we provide a comparative complexomics analysis of leaf whole cell lysate of two rice genotypes with contrasting responses to salt using two-dimensional blue native/SDS-PAGE (2D-BN/SDS-PAGE). We aimed to identify changes in subunit composition and stoichiometry of protein complexes elicited by salt. Using mild detergent for protein complex solubilization, we were able to identify 9 protein assemblies as hetero-oligomeric and 30 as homo-oligomeric complexes. A total of 20 proteins were identified as monomers in the 2D-BN/SDS-PAGE gels. In addition to identifying known protein complexes that confirm the technical validity of our analysis, we were also able to discover novel protein-protein interactions. Interestingly, an interaction was detected for glycolytic enzymes enolase (ENO1) and triosephosphate isomerase (TPI) and also for a chlorophyll a-b binding protein and RuBisCo small subunit. To show changes in subunit composition and stoichiometry of protein assemblies during salt stress, the differential abundance of interacting proteins was compared between salt-treated and control plants. A detailed exploration of some of the protein complexes provided novel insight into the function, composition, stoichiometry and dynamics of known and previously uncharacterized protein complexes in response to salt stress.

1. Introduction

Salt stress imposes a major challenge to agricultural production, especially in arid and semi-arid regions, where the soil salt concentration increases with increasing land clearing or irrigation with saline water. Increased soil salt concentration mitigates the ability of plants to take up water and increases the rate of tissue deposition of harmful ions (mainly Na^+ and Cl^-). Therefore, salinity imposes both osmotic and ionic stresses, impairs metabolic and photosynthetic processes, and consequently reduces plant growth and yield production (Munns, 2005; Munns and Tester, 2008). To cope with osmotic effects of salt, plants have evolved adaptive mechanisms to minimize water loss and to actively maintain water uptake (Deinlein et al., 2014). In addition, depending on the extent of their salt tolerance, plants have acquired mechanisms for limiting Na^+ absorption, excluding salt from cells, and sequestering harmful ions into vacuoles in order to avoid their excess accumulation in the cytosol and organelles such as the chloroplast (Munns and Tester, 2008; Negrão et al., 2011). Plants have also evolved mechanisms to minimize adverse side-effects of salt buildup in the cytoplasm including the production and accumulation of compatible solutes such as glycine betaine, proline and sugar terhalose (Munns and Tester, 2008). The ionic stress associated with salinity leads to excess production of ROS (reactive oxygen species), such as superoxide radicals ($O_2^{\bullet}$), hydrogen peroxide (H_2O_2), and hydroxyl radicals ($OH^{\bullet -}$). To minimize the adverse effects of stress-induced ROS production, plants have evolved sophisticated enzymatic and

* Corresponding authors at: (J. Gharechahi) Chemical Injuries Research Center, Baqiyatallah University of Medical Sciences, Tehran, Iran. (GH. Salekdeh) Department of Systems Biology, Agricultural Biotechnology Research Institute of Iran, Agricultural Research, Education, and Extension Organization, Karaj, Iran.
E-mail addresses: jgharechahi@gmail.com (J. Gharechahi), hsalekdeh@yahoo.com (G.H. Salekdeh).

http://dx.doi.org/10.1016/j.jplph.2016.05.023
0176-1617/

non-enzymatic mechanisms to maintain the production of ROS under tight control (Apse and Blumwald, 2002; Munns and Tester, 2008).

The mechanism of adaptation to salt stress is a complex process that needs to be inspected at global physiological, cellular, and biochemical levels in order to obtain an integrated systems view of salinity tolerance. This complex phenomenon ultimately needs coordinated reprogramming of metabolic and regulatory processes that almost exclusively depends on changes in gene expression and is usually orchestrated by an array of changes in protein abundance, modifications, interactions, and subcellular localization. Nearly all catalytic and regulatory processes in living organisms are executed and controlled by proteins that act in a cooperative manner. Indeed, proteins rarely function as single entity, but rather they execute their tasks through interactions with other proteins or molecules. The majority of proteins are thought to participate in multiple cellular processes, and this multi-functionality is possible through interactions with other molecules (Miteva et al., 2013). In addition, most proteins assemble into large macromolecular complexes to accomplish essential cellular tasks such DNA replication, transcription, ATP synthesis, and photosynthesis. It is now well documented that the catalytic and regulatory activities of proteins are, to a large extent, controlled through dynamic physical or functional protein-protein interactions (Drewes and Bouwmeester, 2003). Therefore, without knowledge about protein-protein interactions, it would not be possible to fully understand the functions of proteins in their cellular context. Characterization of these interactions is thought to be essential for understanding the biology of a plant system in reaction to abiotic and biotic stresses.

The study of protein-protein interactions is not trivial since they are inherently dynamic, weak, and short lived in nature (Miteva et al., 2013). One approach is to isolate protein complexes in their native conformations and to identify their interacting proteins using mass spectrometry. This is routinely being done using tandem affinity purification (TAP) and co-immunoprecipitation (co-IP), both of which are relatively labor intensive and are only able to recover interacting partners of a single protein at a time (Drewes and Bouwmeester, 2003; Gavin et al., 2002; Rigaut et al., 1999). In addition to their dependence on transgene technology and the requirement for specific antibodies, by using such techniques it is not always straightforward to discriminate between separate protein assemblies that share same protein partners (Remmerie et al., 2009). In addition, these approaches do not provide a global picture of protein-protein interactions in a complex proteome and do not allow the evaluation of the isolated complexes in terms of their cellular abundance. However, the two-dimensional blue native/SDS-PAGE (2D-BN/SDS-PAGE) method coupled with mass spectrometry for protein identification represents an interesting alternative technique that allows us to recover, separate, quantitatively measure, and identify protein complexes of varying sizes (10–10,000 kDa) under native conformation (Eubel et al., 2005; Schagger et al., 1994). With the introduction of mild non-ionic detergents for protein solubilizastion, this technique has allowed gentle isolation of both intact soluble and extremely hydrophobic membrane-bound protein complexes (Eubel et al., 2005). Additionally, the 2D-BN/SDS-PAGE method enables the study of protein complexes in terms of changes in protein-protein interactions, subunit composition, stoichiometry, and post translational modifications provoked by a stressor to an organism. The 2D-BN/SDS-PAGE also displays some technical limitations, such as dependency on the staining properties of individual proteins, ambiguity in assigning the identified proteins to the spots or complexes, limited size resolution, and inability to separate transient complexes and those with weak interactions (Muller et al., 2015). The 2D-BN/SDS-PAGE was first introduced for the separation and identification of mitochondrial and chloroplast membrane protein complexes (Eubel et al., 2005; Schagger, 2006; Schagger et al., 1994; Schägger and von Jagow, 1991). However, with some technical improvements it has been utilized for the isolation and exploration of whole cell lysate complexes (Camacho-Carvajal et al., 2004; Remmerie et al., 2009; Shekari et al., 2011).

As an important cereal crop and staple food, rice is a salt-sensitive plant with its growth and productivity significantly affected by salinity (Negrão et al., 2011). Rice could only tolerate salinities within the range of 1.9–3 dS/m and under salinities exceeding 6 dS/m it may experience up to 50% reduction in yield (Grattan et al., 2002; Linh le et al., 2012). There exists a high degree of variability in terms of salt stress tolerance among cultivars and landraces of rice. Interestingly, cultivars with high salt tolerance inevitably suffer from poor agronomic traits such as tall plant stature, photosensitivity, poor grain quality, and low yield (Walia et al., 2005). Traditional tolerant genotypes have been frequently used as donors of salt tolerance genes in rice breeding programs for salt stress tolerance. As an example, FL478 is a recombinant inbred line (RIL) that was generated from the cross of a traditional *indica* landrace, Pokkali, as salt-tolerant parent and IR29 (Bonilla et al., 2002). The IR29 is an improved *indica* cultivar, which is frequently used as a standard genotype for salt sensitivity. It suffers mainly from excess accumulation of Na^+ in the photosynthetic tissues and loss of growth under salinity (Hosseini et al., 2015). FL478 was selected for salt stress tolerance and displayed higher or comparable degrees of salt tolerance compared to the Pokkali, but showed greater tillering capacity, which is an important characteristic for maintaining yield under salinity conditions (Gregorio et al., 2002; Walia et al., 2005; Zeng and Shannon, 2000). Similar to the Pokkali, the salt tolerance phenotype of FL478 is also largely attributed to its higher capacity for maintaining low ionic balance (Na^+ to K^+ ratio) in photosynthetic tissues and its faster growth under saline conditions (Walia et al., 2005).

To show whether changes in protein complexome contribute to salt tolerance/sensitivity or whether salt stress promotes any changes in stoichiometry of protein complexes, we analyzed the whole cell lysate complexes of FL478 and its salt-sensitive parent IR29. Our results, for the first time, provide insight into the salt-induced changes in the complexome of two rice genotypes with a close genetic background and different susceptibility to salt stress.

2. Material and methods

2.1. Plant material and salt stress treatment

Seeds of two rice genotypes, FL478 and IR29, were obtained from the International Rice Research Institute, IRRI (Los Baños, Pillippines). Seeds were surface sterilized and germinated on moisturized filter papers under dark condition. Four day old seedlings were fixed in holes of a styrofoam board (two seedlings in each hole) with the net at the bottom and floated on rectangular 18 L hydroponic tanks filled with the Yoshida nutrient solution (Yoshida et al., 1976). The nutrient solution was changed every 7 days and the pH was monitored daily and maintained at 5.0, by adding either 1 N NaOH or HCl. Plant seedlings were allowed to grow under controlled growth chamber condition for 21 days. Before imposing salt stress, weak or off-type seedlings were removed to ensure uniformity at the start of the experiment. The 25-day old seedlings were subjected to salt stress by adding 100 mM NaCl to the nutrient solution. Plants were let to grow under saline and control (nutrient solution without NaCl) conditions for additional 12 days. The saline nutrient solution was changed every two days to maintain a constant salt concentration. The experiment was conducted under a completely randomized design with two salinity conditions (0 and 100 mM NaCl) and two genotypes (IR29 and FL478) under three

biological replications. At the end of the experiment, seedlings were carefully pulled out from the culture trays and washed thoroughly with distilled water to remove salts from the surface. The main shoot and root was harvested by cutting at the base of the stem or crown. Leaf samples were collected from healthy and fully expanded leaves and immediately frozen in liquid nitrogen and stored at −80 °C for later analysis.

2.2. Root and shoot fresh and dry weights

The effect of salt stress on total biomass production was assessed by measuring the total shoot and root fresh weight (FW) and dry weight (DW) of salt-stressed and control plants. Immediately after harvest, root and shoot samples were weighed to record their FW. For DW measurement, roots and shoots were weighted, separately, oven dried at 75 °C for 72 h, and weighed again.

2.3. Determination of Na^+ and K^+ concentration

To determine the extent of Na^+ accumulation and to estimate the balance between Na^+ and K^+ in salt-treated and control plants, the total root and shoot content of Na^+ and K^+ and the ratio of K^+ to Na^+ were measured. Plant materials (shoot and root) were ground in liquid nitrogen to a fine powder using mortar and pestle. The resulting powder was oven-dried at 75 °C for 72 h. Dried materials (300 mg) were processed by adding 10 mL of 500 mM nitric acid (HNO_3) and incubating at 80 °C for at least 2 h in a water bath. The resulting solution was filtered to remove shoot or root particulates. The concentration of Na^+ and K^+ was measured in diluted (1:10 v/v) samples using atomic absorption spectrophotometer (AAS 3100, PerkinElmer, USA). Na^+ and K^+ concentrations are presented on the basis of mmol per gr DW.

2.4. Protein extraction

Sample preparation was carried out as previously described by Wittig et al. (2006). Briefly, 200 mg of fresh leaf samples were ground in liquid nitrogen using mortar and pestle and the resulting powder was resuspended in 250 μL of lysis buffer (50 mM imidazol, 50 mM NaCl, 2 mM 6-aminohexanoic acid, and 1 mM EDTA, pH 7.0) supplemented with 3% dodecyl-β-D-maltoside (DDM) and complete protease inhibitor cocktail (Sigma, St. Louis, MO). The mixture was gently mixed and incubated on ice for 2 h followed by a centrifugation at 15000*g* and 4 °C for 15 min. The supernatant was collected and subjected to an additional centrifugation step at 20000*g* and 4 °C for 20 min. Finally, the supernatant was collected and 10 μL of a 50% glycerol stock solution was added and the samples were then snap frozen in liquid nitrogen and stored at −70 °C until being used for the BN-PAGE analysis. The protein concentration was determined by the Bradford assay using IgG as a standard.

2.5. Two-dimensional BN/SDS-PAGE

BN-PAGE was performed as described previously with slight modifications using a Hoefer™ SE250 electrophoresis unit (GE Healthcare) (Shekari et al., 2011; Wittig et al., 2006). A total of 1400 μg protein was loaded into each lane of a BN-PAGE gel consisting of 3.5% stacking and 5–14% gradient resolving gel. The anode (25 mM imidazole with pH 7.0) and the cathode buffer (50 mM tricine and 7.5 mM imidazole with pH 7.0, supplemented with 0.02% w/v coomassie brilliant blue (CBB) G250) were chilled at 4 °C before use. Electrophoresis was started at 150 V for 30 min and then adjusted to 20 mA for 10 h. The molecular weight (MW) of complexes was estimated by co-electrophoresis of a high-MW Calibration Kit for native electrophoresis (GE Healthcare) with size range of 660, 440, 232, 140 and 66 kDa. For the second dimension, lanes of the first dimension BN-PAGE were cut out and equilibrated in denaturing buffer (2% w/v SDS, 66 mM Na_2CO_3, 0.67% β-mercaptoethanol) for 20 min and then fixed separately on the top surface of the SDS-PAGE gels using 0.5% agarose. SDS-PAGE was performed using a 10% stacking and a 12% resolving gel according to the Schagger protocol (Schagger, 2006). Gels were stained with a CBB staining solution containing 0.02% CBB-G250 in 2% (w/v) phosphoric acid, 5% aluminum sulfate and 10% ethanol (Kang et al., 2002).

2.6. Image acquisition and data analysis

CBB-stained gels were scanned using a GS-800 calibrated densitometer (Bio-Rad, Hercules, CA) at a resolution of 600 dots per inches. The scanned gels were saved as raw TIFF images. Spot detection and protein quantification were carried using the Image Master™ 2D Platinum software version 6.0 (GeneBio, Geneva, Switzerland). Spots were manually matched and reproducibly detected spots in different treatments were labeled with unique spot IDs. To identify differentially abundant proteins, the percentage volume (%vol) of each spot was extracted and used as normalized quantitative value of that spot.

2.7. Protein identification and database search

Protein spots were manually excised from the second dimension SDS-PAGE gels. Gel plugs were destained for 1 h at room temperature using a solution containing 50 mM ammonium biocarbonate (NH_4HCO_3) in 100% acetonitrile (50:50 v/v). The solution was removed and gel pieces were left to dry for 30 min at 37 °C. Proteins in the gel pieces were digested in 10 μL solution of modified trypsin (12 ng/μL trypsin in 50 mM ammonium bicarbonate) for 45 min at 4 °C. Excess trypsin solution was removed and gel pieces were overlaid with 50 mM NH_4HCO_3 for overnight incubation at 37 °C. After centrifugation, a one μL aliquot of each peptide mixture was applied directly to the ground steel MALDI target plate, then an equal volume of freshly prepared 5 mg/mL solution of 4-hydroxy-α-cyano-cinnamic acid (Sigma) in 50% aqueous (v/v) acetonitrile containing 0.1%, trifluoroacetic acid (v/v) was added. Positive-ion MALDI mass spectra were obtained using a Bruker ultraflex III in reflectron mode, equipped with a Nd:YAG smart beam laser. MS spectra were acquired over a mass range of *m/z* 800–4000. Final mass spectra were externally calibrated against an adjacent spot containing 6 peptides (des-Arg1-Bradykinin, 904.681; Angiotensin I, 1296.685; Glu1-Fibrinopeptide B, 1750.677; ACTH (1–17 clip), 2093.086; ACTH (18–39 clip), 2465.198; ACTH (7–38 clip), 3657.929). Monoisotopic masses were obtained using a SNAP averaging algorithm (C 4.9384, N 1.3577, O 1.4773, S 0.0417, H 7.7583) and a signal-to-noise ratio (S/N) threshold of 2. For each spot the ten strongest peaks of interest, with an S/N greater than 10, were selected for MS/MS fragmentation. Fragmentation was performed in LIFT mode without the introduction of a collision gas. The default calibration was used for MS/MS spectra, which were baseline-subtracted and smoothed (Savitsky-Golay, width 0.15 *m/z*, cycles 4); monoisotopic peak detection used an SNAP averaging algorithm (C 4.9384, N 1.3577, O 1.4773, S 0.0417, H7.7583) with a minimum S/N of 3. Bruker flex analysis software was used to perform the spectral processing and peak list generation for both the MS and MS/MS spectra. Combined mass spectral and tandem mass spectral data were submitted to database searching using a locally-running copy of the Mascot program (Matrix Science Ltd., version 2.1), through the Bruker BioTools interface (version 3.1). Search criteria included: enzyme, trypsin; variable modifications, oxidation (M); fixed modifications, carbamidomethyl (C); peptide toler-

Table 1
Phenotypic characterization of FL478 and IR29 under salinity condition. The response of plants to salt stress (100 mM NaCl) was assessed by measuring the amount of biomass produced under saline and control conditions. The total root and shoot Na^+ and K^+ concentrations were also measured. Data are means of at least three independent biological replications (mean ± se). Duncan's multiple range test was used for mean comparison and grouping. Mean values with the same letter are not statistically significant. Those labeled with different letters are shown significant statistical changes ($p \leq 0.01$).

Trait	IR29		FL478	
	Control	Salt stress	Control	Salt stress
Root and shoot fresh (FW) and dry (DW) weights (g)				
Root FW	1.65 ± 0.20^{b}	1.90 ± 0.08^{b}	3.21 ± 0.45^{a}	2.68 ± 0.57^{ab}
Root DW	0.13 ± 0.01^{a}	0.16 ± 0.004^{a}	0.21 ± 0.03^{a}	0.20 ± 0.04^{a}
Shoot FW	4.71 ± 0.49^{c}	2.81 ± 0.02^{d}	9.01 ± 0.21^{a}	6.50 ± 0.65^{b}
Shoot DW	0.80 ± 0.03^{b}	0.59 ± 0.01^{c}	1.51 ± 0.21^{a}	1.09 ± 0.20^{a}
Na^+ and K^+ concentrations (mmol g^{-1} DW) and K^+ to Na^+ ratio				
Root K^+	3.61 ± 0.3^{a}	0.98 ± 0.13^{c}	0.92 ± 0.05^{c}	1.82 ± 0.1^{b}
Root Na^+	0.68 ± 0.02^{c}	1.3 ± 0.1^{b}	0.86 ± 0.03^{c}	1.66 ± 0.06^{a}
Root K^+/Na^+	5.31^{a}	0.75^{b}	1.07^{b}	1.09^{b}
Shoot K^+	5.2 ± 0.17^{a}	2.65 ± 0.05^{c}	5.12 ± 0.11^{a}	3.99 ± 0.14^{b}
Shoot Na^+	0.62 ± 0.02^{c}	1.29 ± 0.03^{a}	0.57 ± 0.02^{c}	0.99 ± 0.02^{b}
Shoot K^+/Na^+	8.4^{a}	2.05^{b}	8.9^{a}	4.03^{c}

ance, 100 ppm; MS/MS tolerance, 0.5 Da; max missed cleavages, 1; instrument, MALDI-TOF/TOF. The search criteria also included carbamidomethyl (C) as a fixed modification for all alkylated samples. Searches were made against the NCBI protein database (22 Feb 2011, 9,029,658 sequences; 3,093,850,741 residues), taxonomy; *Oryza sativa* (132,605 sequences), using a locally running Mascot version 2.1 (Matrix Science Ltd.). The identity of a protein spot was accepted if its total ion score was greater than 64 at the significance threshold of 95% ($p \leq 0.05$) and had at least two peptide sequences determined.

2.8. Functional annotation and in silico reconstruction of protein complexes

For functional annotation, the sequence of proteins were retrieved from the Uniprot database and subjected to gene ontology (GO) analysis using the Blast2GO software (Götz et al., 2008). Based on the gene ontologies retrieved from the uniprot database, proteins were classified into three high-level GO terms molecular function, biological process, and cellular component. Subcellular localization of proteins was deduced from gene ontologies assigned under high-level GO term cellular component.

For reconstruction of protein complexes, all vertically aligned proteins in the second dimension SDS-PAGE were subjected to the prediction of protein–protein interaction by the Search Tool for the Retrieval of Interacting Genes/Proteins (STRING) database (http://string.embl.de/) (Jensen et al., 2009). To exclude unrelated co-migrating proteins, proteins that showed to interact in BN-PAGE gels were further inspected to be categorized into the same functional ontology under the high-level GO term biological process. This is a general assumption, since proteins that assemble into a given protein complex are likely to be involved in a similar biological process (Remmerie et al., 2011).

2.9. Statistical analysis

All quantitative physiological and proteomic data were subjected to statistical analysis. Considering the two genotypes (IR29 and FL478) and two treatment conditions (control and salinity), four genotype × treatment combinations were analyzed by one-way analysis of variance (ANOVA). The significance statistical threshold was set at 99% ($p \leq 0.01$). Duncan's multiple range test was performed for means comparison. All statistical analyses were carried out using SAS software ver. 9 (SAS Institute, Cary, NC, USA).

3. Results and discussion

3.1. The physiological response of plants to salt stress

To determine whether changes that are observed in the complexome between plants under saline and control conditions are physiologically relevant, some physiological characteristics of plants were evaluated. The differential response of genotypes with differing susceptibility to salt stress is usually assessed by measuring the amount of biomass produced under saline and control conditions (Munns, 2002). Therefore, to ascertain whether our salt stress condition enabled a differential response of contrasting genotypes to salt stress, the total shoot and root fresh and dry weights (FW and DW) as indicators of growth were measured. The total shoot FW was reduced in both genotypes but to a greater extent in the salt-sensitive IR29 (1.67-fold) under salinity conditions (Table 1). However, shoot DW was not affected in the salt-tolerant FL478, while in IR29 the change was statistically significant ($p \leq 0.05$) but the reduction was less than 1.5-fold (Table 1). It should be noted that, under both control and salinity conditions, FL478 produced higher shoot FW and DW than IR29, meaning that FL478 could better dilute the adsorbed salt and reduce the salt concentration in its photosynthetic tissues by producing higher biomass. Root FW and DW were not affected by salinity in both genotypes and the differences in between genotypes were also not significant (Table 1).

The root Na^+ concentration was increased to the same extent (more than 1.9 fold) in both genotypes under salinity (Table 1). However, the total root K^+ concentration was dramatically reduced (more than 3.6 fold) in IR29, and even increased (more than 1.9-fold) in FL478 after exposure to salinity. This resulted in a huge decrease (7-fold) in K^+ to Na^+ ratio in IR29. These results suggested that, under salt stress, the balance between K^+ and Na^+ was largely affected in roots of the salt-sensitive IR29. Shoot Na^+ concentration was increased in both genotypes but to a greater extent in IR29. Shoot K^+ concentration behaved similarly and showed a significant reduction (more than 1.9) in IR29, while the change (1.2-fold decrease) in FL478 was not marked. A greater reduction in the shoot K^+ concentration resulted in a significant perturbation in the balance between K^+ to Na^+ in IR29 under the salinity condition. Due to the importance of K^+ as an essential co-factor for many enzymes, this reduction imposes profound impacts on plant growth and development. Our results showed that the rate of Na^+ accumulation was same for both genotypes. However, the salt-tolerant genotype FL478 maintained a higher level of K^+ in both roots and shoots compared to the salt-sensitive IR29 under the salinity con-

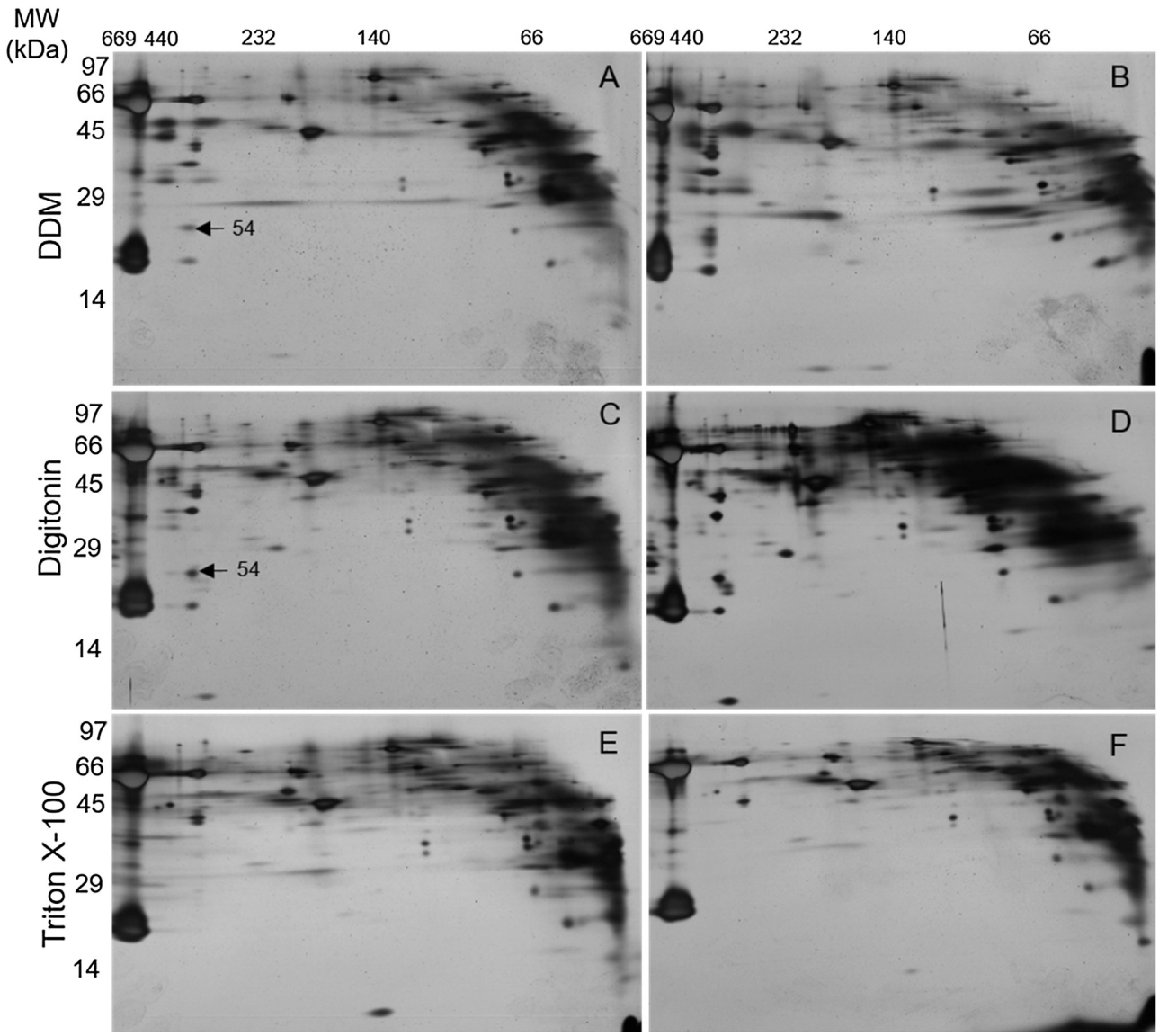

Fig. 1. The effect of three different mild non-ionic detergents each under two extreme concentrations on protein complex solublization in leaf whole cell lysate of rice. A and B show the silver stained 2D-BN/PAGE gel images of whole cell lysate using 1.5 and 3% dodecyl-β-D-maltoside (DDM), respectively. C and D show gel images for 4 and 6% digitonin, respectively. E and F show gel images for 3 and 6% triton X-100, respectively. The final extract concentration and the total amount of protein loaded on each lane of BN-PAGE were equal for each detergent concentration.

dition (Table 1). In addition, FL478 could efficiently sequester the absorbed Na+ in their roots and was therefore better able to physiologically adapt to osmotic stress imposed by salt outside of the roots. Excess accumulation of salt within the plant will almost result in enzyme inhibition, oxidative stresses, disruption of photosynthesis, and loss of growth (Munns and Tester, 2008). Therefore, compared to salt-tolerant FL478, increased growth reduction in the salt-sensitive genotype, IR29, was largely related to the greater salt accumulation that might be either due to its inability to efficiently exclude salt from the transpiration stream and to compartmentalize it into vacuoles or due to leakiness of its roots that allows salt to enter apoplectically (Hosseini et al., 2015).

3.2. The effect of different detergents on protein complex solubilization

Since the type and concentration of detergents significantly affect the success of 2D-BN/PAGE, we first evaluated the effect of three different BN-PAGE-compatible non-ionic detergents each under two different concentrations on protein complexome solubilization. To this end, non-ionic detergents dodecyl-β-D-maltoside (DDM) at concentrations of 1.5 and 3% (w/v), digitonin at concentrations of 4 and 6%, and Triton X-100 at concentrations of 3 and 6% were used for whole cell lysate protein complexome solublization (Fig. 1). As shown in the gel images, the type and concentration of detergent significantly affected the overall pattern of BN-PAGE gels. In gels (Fig. 1A and B) in which proteins were solubilized using DDM, the greatest number of spots with the least background striking were observed. The number of recovered complexes also increased with increasing DDM concentration. When proteins were solubilized using digitonin (Fig. 1C and D), the number of spots displayed in gels were comparable to that for DDM, but they mainly associated with high background streaking that also increased with increasing detergent concentration. Solubilizing proteins using Triton X-100 reduced the number of observed spots on gels and therefore resulted in significant loss of complexes, while increasing its concentration even exacerbated the situation.

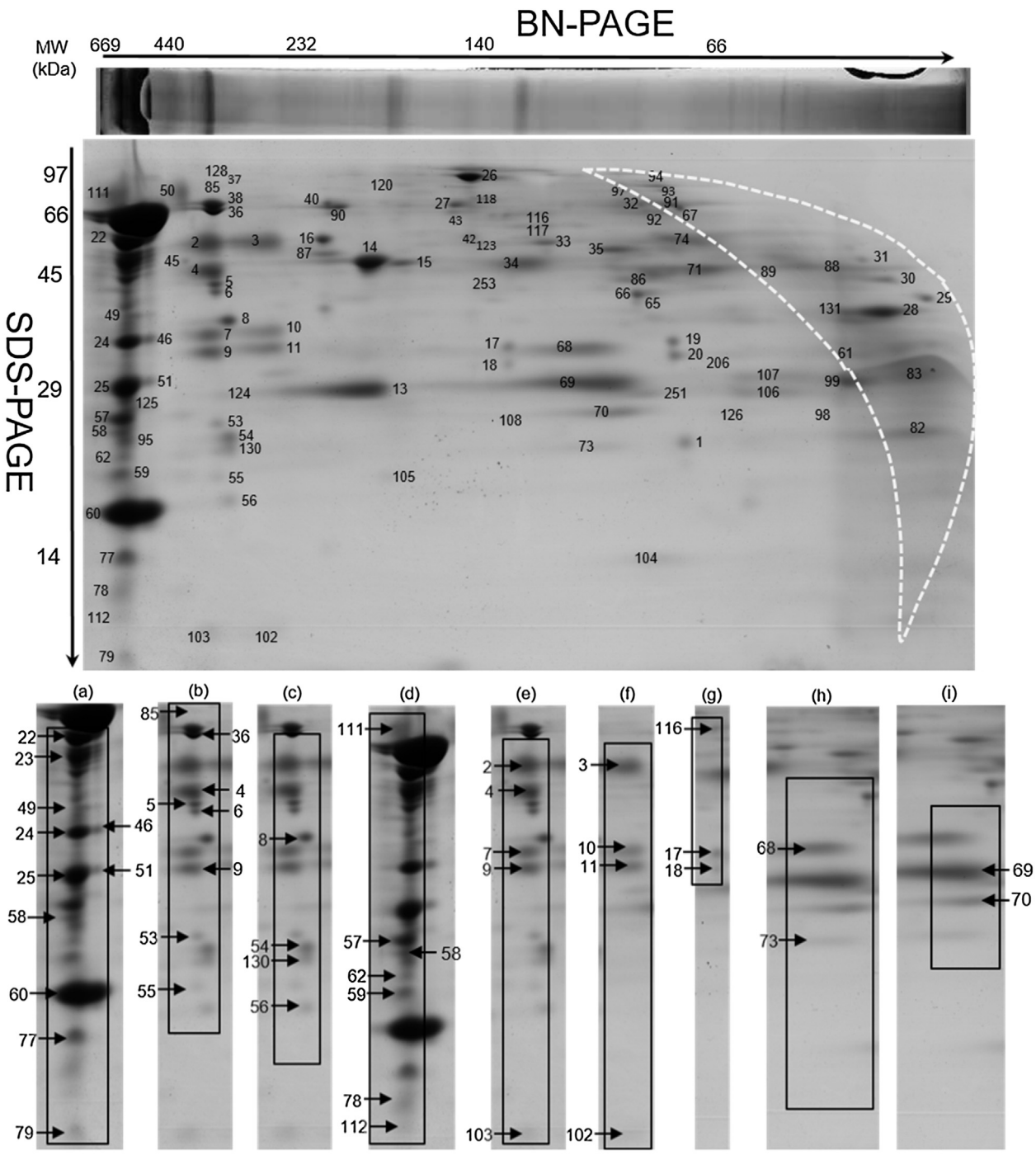

Fig. 2. 2D-BN/PAGE map of the leaf whole cell lysate complexes of rice. Total cell lysate proteins were solubilized in a lysis buffer containing 3% DDM. A total of 1400 μg protein was loaded into a lane of BN-PAGE gel. Proteins in the SDS-PAGE gel were visualized using coomassie brilliant blue (CBB). The identified proteins are labeled with numbers that correspond to spot IDs as reported in Tables 2–4, and supplementary Table 1. Monomeric proteins were mostly resolved in the hyperbolic region of the gel (dashed white line). The spot position of proteins assigned to each of the hetero-multimeric protein complexes (a–i) are shown in cropped gel images. Further details are presented in Table 2.

The presence of cytochrome b6-f complex iron-sulfur subunit (spot 54) can be used as an indicator of extraction since it is easily removed by detergents. In our preliminary test we only detected this protein on gels in which proteins were solubilized using DDM and digitonin. Protein solubilization using Triton X-100 resulted in nearly complete loss of this protein (Fig. 1E and F). Since protein complex solubilization using 3% DDM (Fig. 1B) recovered a greater number of complexes and produced gel images with less background streaking, therefore it was selected for complexome analysis. Supplementary Fig. 1 displays all replicate gel images of FL478 and IR29 under control and saline conditions in which proteins have been solubilized using 3% DDM.

3.3. Protein identification and gene ontology analysis

For protein identification, those unique spots which were reproducibility detected on replicate 2D-BN/PAGE gels were picked and subjected to MS analysis (a total of 130 unique spots). Combined

Table 2
The hetero-multimeric protein complexes identified in this study. Proteins that vertically aligned and showed similar shape were considered as candidate interacting proteins.

Com	Spot ID[a]	Protein Name	Accession number	Gene name	1D-MW[b]	2D-MW[c]	The MW[d]
a	22	Ribulose bisphosphate carboxylase large chain	E9KIP7	rbcL	556	47	52.7
	23	Ribulose bisphosphate carboxylase large chain	E9KIP7	rbcL	556		
	24	Ribulose bisphosphate carboxylase large chain	E9KIP7	rbcL	556	33	52.7
	25	Ribulose bisphosphate carboxylase large chain	P0C512	rbcL	556	30	52.8
	49	Ribulose bisphosphate carboxylase large chain	P0C512	rbcL	556	40	52.8
	46	Ribulose bisphosphate carboxylase large chain	P0C512	rbcL	548	40	52.8
	51	Ribulose bisphosphate carboxylase large chain	P0C512	rbcL	548	30	52.8
	58	Ribulose bisphosphate carboxylase large chain	Q5K3B1	rbcL	563	23	52.7
	60	Ribulose bisphosphate carboxylase small chain	Q0INY7	rbcs	537	17	19.6
	77	Ribulose bisphosphate carboxylase large chain	E9KIP7	rbcL	559	14	52.7
	79	Ribulose bisphosphate carboxylase large chain	Q37247	rbcL	557	9	45.1
b	5	ATP synthase gamma chain	A2YLT1	atpG	336	40	39.6
	4	ATP synthase subunit alpha, chloroplastic	P0C2Z6	atpA	343	43	55.6
	6	ATP synthase gamma chain	A2YLT1	atpG	336	39	39.6
	9	ATP synthase subunit alpha, chloroplastic	P0C2Z5	atpA	344	32	55.6
	36	ATP synthase subunit beta, chloroplastic	P12085	atpB	340	55	53.9
	53	ATP synthase subunit alpha	Q8S7T5	atpA	333	24	55.1
	55	ATP synthase subunit alpha, chloroplastic	P0C2Z6	atpA	332	20	55.6
	85	ATP synthase subunit alpha, chloroplastic	P0C2Z6	atpA	340	63	55.6
c	8	Cytochrome f	P0C389	petA	314	35	35.4
	54	Cytochrome b6-f complex iron-sulfur subunit	Q69S39	petC	312	22	23.8
	56	Cytochrome b6-f complex subunit 4	P0C319	petD	313	17	19
	130	Cytochrome b6	P12123	petB	312	21	24.1
d	57	Photosystem I reaction center subunit II	Q84PB4	psaD	563	25	22
	58	Chlorophyll a-b binding protein P4	A0A067K589	–	563	23	27.6
	59	Photosystem-1F subunit	Q9ZSU5	psaF	572	19	24.7
	62	Photosystem I reaction center subunit IV	Q6Z3V7	psaE	562	21	15.5
	78	Photosystem I reaction center subunit VI	Q0DG05	psaH	569	12	15
	111	Photosystem I P700 chlorophyll a apoprotein A2	P0C358	psaB	587	87	82.5
	112	Photosystem I iron-sulfur center	P0C361	psaC	572	11	8.9
e	2	Photosystem II 47 kDa protein	Q6ENE8	psbB	348	48	56.1
	4	Photosystem II CP43 reaction center protein	P0C365	psbC	343	43	52
	7	Putative photosystem II D2 protein	Q108X8	psbD	347	34	31.2
	9	Photosystem II protein D1	P0C434	psbA	344	32	38.9
	103	Photosystem II reaction center protein H	P0C422	psbH	350	10	7.8
f	3	Photosystem II 47 kDa protein	Q6ENE8	psbB	247	48	56.1
	10	Putative photosystem II D2 protein	Q108X8	psbD	239	34	31.2
	11	Photosystem II protein D1	P0C434	psbA	241	33	38.9
	102	Cytochrome b559 subunit alpha	P0C370	psbE	246	10	9.4
g	17	Triosephosphate isomerase	P48494	TPI	122	33	27
	18	Triosephosphate isomerase	P48494	TPI	122	32	27
	116	Enolase	Q42971	ENO1	121	54	47.9
h	68	Chlorophyll a-b binding protein	Q53N83	–	98	33	30.2
	73	Ribulose bisphosphate carboxylase small chain	Q0INY7	rbcs	92	22	19.6
i	69	Chlorophyll a-b binding protein of LHCII type III	Q6ZF30	–	92	30	28.7
	70	Chlorophyll a-b binding protein	Q7XV11	–	92	26	27

[a] The number assigned to each spot during gel images analysis.
[b] The molecular weight of the spot as calculated from its migration in the BN-PAGE gel.
[c] The molecular weight of the spot based on its migration in the SDS-PAGE gel.
[d] The theoretical molecular weight of the protein in the uniprot database.

peptide mass fingerprinting (MS) and MS/MS analysis resulted in identification of 110 proteins (Supplementary Table 1 and Fig. 2). Interestingly, five spots were identified to contain multiple proteins. These include spots 4, 9, 58, 83, and 106, which all were identified as containing two distinct proteins (Fig. 2 and Supplementary Table 1). Since identification of multiple proteins in a single 2-DE spot impedes proper quantification of target protein, we excluded these spots from the list of up/down regulated proteins. Analysis of subcellular localization of the identified proteins suggest that 29% are known to localize in chloroplast thylakoid membrane, 15% in chloroplast stroma, 12% in chloroplast envelope, 11% in mitochondria, 6% in cytosol, and the remaining are belonging to other organelles found in the cells.

3.4. Reconstruction of protein complexes

In a typical 2D-BN/SDS-PAGE gel, interacting proteins belonging to a single protein complex co-migrate during the first dimension (BN-PAGE) and then separate in the second dimension (SDS-PAGE) based on their molecular weight into vertically aligned spots with almost similar shape (Lasserre et al., 2006). However, it should be noted that co-migrating proteins may not necessarily interact physically, since multiple combinations of different protein complexes may co-migrate during the first dimension (Reisinger and Eichacker, 2007). Therefore, for reconstruction of protein complexes, those vertically aligned spots that also displayed the same shape were further inspected for protein-protein interactions using the STRING database. In addition, to show whether the predicted

Table 3
Homo-oligomeric protein complexes identified in this study.

Spot ID[a]	Protein Name	Accession number	1D-MW[b]	2D-MW[c]	The MW[d]	Oligomerization state
105	Nucleoside diphosphate kinase 1	Q07661	173	19	16.8	decamer
27	Dihydrolipoyl dehydrogenase	Q9ASP4	138	58	52.6	dimer
19	Triosephosphate isomerase	Q69K00	70	33	32.3	
20	Triosephosphate isomerase	Q69K00	70	32	32.3	
26	Putative transketolase 1	Q5VNW1	134	105	68.8	
34	Photosystem II CP43 reaction center protein	P0C365	117	44	52	
35	Phosphoribulokinase	Q6Z8F4	88	47	44.8	
42	Putative transketolase 1	Q5VNW1	134	50	68.8	
65	Putative inorganic pyrophosphatase	Q6ZGJ8	76	35	31.7	
66	Osjnba0076n16.12 protein	Q7X7H3	81	40	39.4	
86	Sedoheptulose-1,7-bisphosphatase	Q84JG8	86	41	42.2	
92	Alanine aminotransferase	Q84UX4	79	54	53.5	
106	Carbonic anhydrase	B7E5F1	51	29	22.1	
107	Carbonic anhydrase	O80422	49	31	29.1	
117	Isocitrate dehydrogenase	A0A0D9YCK0	114	51	52.6	
118	Acetohydroxy-acid reductoisomerase	Q65XK0	138	60	62.3	
123	Succinyl-CoA ligase [ADP-forming] subunit beta	Q6K9N6	131	47	45	
126	Susceptibility homeodomain transcription factor	Q8SAA7	58	26	12.7	
43	Putative alanine aminotransferase	Q69UU3	138	54	53.6	
95	Aminomethyltransferase	Q7XPR2	563	22	43.9	docedamer
13	Chlorophyll a-b binding protein, chloroplastic	Q10HD0	185	30	28.4	hexamer
87	Fructose-bisphosphate aldolase	I1Q3J5	205	46	41.3	
104	Cytochrome b5	Q6K680	75	13	10.8	
14	Fructose-bisphosphate aldolase	Q2RA00	183	44	41.6	pentamer
16	Glutamine synthetase, Chloroplastic	P14655	207	48	46.6	
15	Fructose-bisphosphate aldolase	Q2RA00	166	44	41.6	tetramer
37	Malic enzyme	Q9FRT2	304	95	65.4	
38	Catalase isozyme A	Q0E4K1	304	70	56.6	
40	Adenosylhomocysteinase	Q84VE1	201	63	53.2	
1	Putative superoxide dismutase [Cu-Zn]	P93407	66	22	21.3	trimer
33	Putative hydroxypyruvate reductase	Q6YU90	110	48	42	

[a] The number assigned to each spot during gel images analysis.
[b] The molecular weight of the spot as calculated from its migration in the BN-PAGE gel.
[c] The molecular weight of the spot based on its migration in the SDS-PAGE gel.
[d] The theoretical molecular weight of the protein in the uniprot database.

Table 4
Monomeric proteins identified in this study.

Spot ID[a]	Protein Name	Accession number	1D-MW[b]	2D-MW[c]	The MW[d]
28	33 kDa oxygen evolving protein of photosystem II	Q943W1	35	36	34.8
29	Uncharacterized protein	I1QKC5	33	38	33.2
30	Chloroplast 28 kda ribonucleoprotein	Q650W6	35	41	35.4
31	Putative uncharacterized protein	B9G0N8	38	45	47.6
61	ATP synthase subunit beta, chloroplastic	P12085	42	32	53.9
67	Putative alanine aminotransferase	Q69UU3	69	58	53.6
71	Putative uncharacterized protein	B8BPB7	63	43	41
74	Aminomethyltransferase	Q7XPR2	64	48	43.9
82	Oxygen-evolving enhancer protein 3	Q0D5P8	33	24	22.9
83	Photosystem II oxygen-evolving complex protein 2	Q8GTK4	33	31	26.9
88	Putative uncharacterized protein	B8BPB7	42	43	41
89	Putative uncharacterized protein	B8BPB7	48	43	41
91	ATP synthase subunit beta	B9EYN3	69	55	51.7
93	Protein disulfide isomerase-like 1-1	Q53LQ0	75	85	56.8
94	Phosphoglucomutase, cytoplasmic 2	Q9AUQ4	75	95	62.9
97	Phosphoglucomutase, chloroplast precursor	Q33AE4	87	88	66.1
99	2-Cys peroxiredoxin BAS1	Q6ER94	41	30	28
120	Ferredoxin-dependent glutamate synthase, chloroplastic	B8B5I7	162	90	175
131	33 kDa oxygen evolving protein of photosystem II	Q943W1	41	36	34.8
32	Vacuolar ATPase B subunit	Q7FV25	80	61	54

[a] The number assigned to each spot during gel images analysis.
[b] The molecular weight of the spot as calculated from its migration in the BN-PAGE gel.
[c] The molecular weight of the spot based on its migration in the SDS-PAGE gel.
[d] The theoretical molecular weight of the protein in the uniprot database.

partners of a given protein complex are functionally related, GO annotation data were taken into account. Using these criteria, we could identify 39 protein complexes, of which 9 were identified as hetero-multimers (Table 2) and 30 as homo-multimers (Table 3). In addition, a total of 20 proteins were identified as monomers (Table 4).

3.5. Hetero-multimeric protein complexes

Among the heteromultimeric protein assemblies, RuBisCo, chloroplastic ATP synthase, cytochrome b_6f, and photosystem I and II were identified as known protein complexes. Identification of protein complexes of known identity showed the technical validity of our analysis. RuBisCo is a large and high abundant protein

complex that assembles from 8 large and 8 small catalytic subunits and is found in a hexadecameric structure, L8S8 (Andersson and Backlund, 2008). In this study, from the BN-PAGE gels (first dimension, 1D), RuBisCo was identified as an intact protein complex that focused at the MW ~540–560 kDa which is consistent with its theoretical MW (Fig. 2). During the second dimension SDS-PAGE (2D), the small subunit was detected at its exact MW (~19 kDa) but the large subunit was subjected to extensive degradation and detected in multiple spots (spots 24, 49,46, 22, 23, 25, 51, 79, 77, and 58) at different MW size ranges (9–47 kDa). This degradation was observed under control and salt stress conditions and in both salt-sensitive (IR29) and salt-tolerant (FL478) genotypes, which is in agreement with our previous observations in 2-DE proteomic analysis of rice (Ghaffari et al., 2014; Hosseini et al., 2015). Therefore, this degradation was not the consequence of salt stress treatment and might be occurred during processing BN-PAGE gels for the SDS-PAGE analysis. It seems degradation occurs randomly at sites along the length of RuBisCo large subunit that are prone to degradation.

The chloroplastic ATP synthase (CF0F1) is a large multi-subunit protein assembly that is located in the thylakoid membrane. It catalyzes the synthesis of ATP from ADP and inorganic phosphate by utilizing the electrochemical proton gradient established during photosynthetic electron transport chain (McCarty et al., 2000). Eight spots which were found to be aligned were identified as subunits of CF1 component of the CF0F1 complex (five spots 4, 9, 55, 53, and 85, as alpha, spot 5 and 6 as gamma, and spot 36 as beta subunit). They were detected at the MW 330–340 kDa in the BN-PAGE gels. Spots 9, 53 and 55 were detected far below the theoretical MW of the alpha subunit and therefore might be the product of proteolytic degradation. In fact, this proteolytic degradation is thought to have occurred at specific sites along the length of the protein, since the degradation products were accumulated in reproducibly detected spots. In addition, the alpha subunit (spots 4 and 9) was found to have co-migrated with psbA and psbC as component of photosystem II in SDS-PAGE gels and detected in same spots (Fig. 2 and Table 2). The intact CF1 section of the chloroplastic ATP synthase is a heteromultimers of five polypeptides in a stoichiometry of $\alpha_{3\beta3}\gamma\delta\varepsilon$ (Groth and Pohl, 2001). It is hydrophilic in nature and associates with the membrane through interactions with the transmembrane CF0 component (McCarty et al., 2000). Based on its migration in the BN-PAGE gel and the absence of delta and epsilon subunits, the identified complex represents a partial CF1 complex. The absence of delta and epsilon subunits in the 2D-BN/SDS-PAGE gels might be explained in part due to the stoichiometry of different subunits in the complex or the instability of the complex during sample preparation (Lasserre et al., 2006).

In the SDS-PAGE gels, four vertically aligned spots (spots 54, 130, 56, and 8) were identified as large subunits of cytochrome b6f complex (Cyt b_6f), which is one of the four major integral thylakoid membrane complexes. This complex is involved in photosynthetic electron transfer between the two photosynthetic reaction center complexes (II and I) (Nelson and Yocum, 2006). In the BN-PAGE gels, it was found as a 312 kDa protein complex. The Cyt b_6f complex is composed of four large (PetA, PetB, PetC, and PetD) and four small subunits (PetG, PetL, PetM and PetN) and functions as dimeric complex. Based on its migration in the BN-PAGE gels, it was detected as an intact protein complex, but its small subunits were not detected on gel. The absence of small subunits in the 2D gels might be due to their small size (3–4 kDa) that hinders their detection on a 12% polyacrylamide gel.

Seven vertically aligned spots, which were positioned at the relative MW 560–580 kDa, were identified as subunits of photosystem I (PSI) complex including PsaE (spot 62), PsaD (spot 57), PsaH (spot 78), PsaF (spot 59), PsaC (spot 112), PsaB (spot 111), and a chlorophyll a-b binding protein (spot 58). The exact subunit composition of the PSI complex has yet to be defined but twelve Psa subunits (PsaA-PsaL) and light-harvesting, Chl-binding protein (LHC) LHCa1, LHCa2, LHCa3, and LHCa4 have been proven to be genuine subunits of plant PSI (Nelson and Yocum, 2006). Similarly, five vertically aligned spot within the MW range 340–350 kDa were identified as subunits of photosystem II complex (PSII) including PsbC (spot 4), PsbA (spot 9), PsbD (spot 7), PsbB (spot 2), and PsbH (spot 103). A part of PSII complex was also identified at MW range 240–250 kDa including subunits of PsbD (spot 10), PsbA (spot 11), PsbE (102), and PsbB (spot 3). In addition, we found that PsaB (spot 50) and PsbC (spot 45) subunits localized at MW 390–396 kDa but since their spot shapes were different they may co-migrated during BN-PAGE analysis and did not physically interact. This multiple migration during the first dimension might be due to the dissociation of interacting subunits of a large complex into sub-complexes of similar sizes at domains that show weak interactions.

Two vertically aligned spots with almost similar shape were localized at MW 90 kDa in 1D gels and were identified as chlorophyll a-b binding protein of LHCII type III (LHBC, spot 68) and RuBisCo small subunit (rbcs, spot 73). This suggests that they may interact as heterotetrameric proteins with a stoichiometry of 2LHBC-2rbcs. In addition, it has been shown that these proteins are co-expressed and their gene expression has proven to be under the control of light (Wehmeyer et al., 1990). Since both are chloroplastic proteins that are involved in photosynthesis carbon assimilation, this interaction makes sense. An interaction was also detected between two chlorophyll a-b binding proteins (spots 69 and 70).

Enolase (ENO1, spot 116), an essential enzyme involved in the glycolytic pathway by catalyzing the conversion of 2-phosphoglycerate (2-PGE) to phosphoenolpyruvate (PEP), was found to interact with triosephosphate isomerase (TPI, spots 17 and 18), another enzyme of the glycolytic pathway that catalyzes the reversible conversion of dihydroxyacetone phosphate to glyceraldehyde 3-phosphate. This interaction might be part of a larger metabolon that forms to enhance substrate channeling between glycolytic enzymes. A metabolon is formed by association of sequential enzymes of a particular metabolic pathway into a large protein complex to enable direct channeling of metabolite intermediates between enzymes and to improve catalytic efficiency of the pathway (Sweetlove and Fernie, 2013). It has been shown, at least in *Arabidopsis thaliana*, that glycolytic enzymes associate with mitochondrial membrane through direct protein-protein interactions with mitochondrial outer membrane protein VDAC and form metabolon to supply enough pyruvate for respiration and to restrict the use of intermediate metabolites by other competing pathways (Graham et al., 2007).

3.6. Homo-multimeric protein complexes

In this study, several proteins were identified to localize at MWs greater than their theoretical MWs. For example, spot 38 was identified as catalase isozyme A (CATA). In the BN-PAGE gels it focused at MW 300 kDa and in the SDS-PAGE gels it migrated at around 70 kDa, which clearly indicates that it is a homo-tetrameric protein. Indeed, CATA is a homo-tetramer of four identical polypeptides with a theoretical MW 56 kDa each containing a single heme group (Ray et al., 2012). Change in gel migration of a protein during electrophoresis (gel shifting) may be due to either conformational changes due to sequence variations or post-translational modifications (PTMs) (Shi et al., 2012). In addition, solubilization of subunits of a given protein complex during equilibration step is a critical factor that affects relative migration in the SDS-PAGE gel.

Similarly, spot 37 was identified as malic enzyme with theoretical MW 65 kDa. It migrated as a complex with relative MW 300 kDa in 1D gels and was then found in a spot at MW 100 kDa in the second dimension. It seems that, in the second dimension, the malic

enzyme migrated as a dimeric protein. Indeed, the malic enzyme is a homo-tetrameric protein consisting of two less tightly associated dimers. This means that the interface that connects two monomers to form dimers is much stronger than that of the tetramer interface (Hsieh et al., 2009). Likewise, transketolase 1 was migrated as dimeric (TKT, spot 26) and monomeric protein (spot 42) in the second dimension, SDS-PAGE. This may have resulted from insufficient solubilization during equilibration of BN-PAGE gels for the second dimension. In plants, TKT is a homodimer enzyme essential for the Calvin cycle (Gerhardt et al., 2003).

Some homo- and hetero-multimeric protein complexes were found to migrate at different locations in the BN-PAGE gels representing different oligomerization state of a same protein complex. Additionally, a single protein may associate with different protein complexes of varying molecular masses and therefore be identified in different horizontally aligned spots. For example, as noted above, TPI was found to interact with ENO1. We also identified TPI as single dimeric protein (spot 19 and 20) in the BN-PAGE gels at MW 70 kDa. Fructose-bisphosphate aldolase (FBPA) was identified in a spot corresponding to tetrameric form of FBPA (~160 kDa, spot 15), in a highly abundant spot at MW ~190 kDa (spot 14), and in a less abundant spot at ~210 kDa (spot 87). These results suggested that FBPA might be associated with undetectable protein complexes with varying molecular masses. Indeed, FPBA is capable of binding to a variety of proteins for which it's known to play a moonlighting role in the cell (Sherawat et al., 2008). In addition, it is also speculated that FBPA may present in different oligomerization states (i.e. tetrameric, pentameric, and hexameric).

Among the identified homo-oligomers, chloroplastic glutamine synthetase, (GLN2, spot 16) was identified as a pentameric protein complex (~210 kDa). Indeed, based on x-ray crystallography data from maize (Unno et al., 2006) and *Medicago truncatula* (Seabra et al., 2009), it has been suggested that plant GSs are decameric enzymes consisting of two face-to-face oriented pentameric rings. Therefore, the pentameric GS identified in this study corresponds to a single pentameric ring. This suggests that the two pentameric rings had been dissociated before or during BN-PAGE indicating liable interactions between two pentameric rings.

Proteins such as acetohydroxy-acid reductoisomerase (spot 118), isocitrate dehydrogenase (spot 117), sedoheptulose-1,7-bisphosphatase (spot 86), putative inorganic pyrophosphatase (spot 65), and carbonic anhydrase (spot 106 and 107) were identified as dimeric protein complexes.

3.7. Monomeric proteins

Monomeric proteins are generally localized at the end of the BN-PAGE gel and resolved in the hyperbolic region of the second dimension SDS-PAGE gel (Fig. 2). In this study, proteins such as putative alanine aminotransferase (spot 67), 33 kDa oxygen evolving protein of photosystem II (spots 28, 83, and 131), oxygen-evolving enhancer protein 3 (spot 82), chloroplast 28 kDa ribonucleoprotein (spot 30), ferredoxin-dependent glutamate synthase, chloroplastic (spot 120), and 2-Cys peroxiredoxin BAS1 (spot 99) were identified as monomers.

3.8. Differential abundance of proteins during salt stress

We next sought to identify changes in the abundance of proteins in the two tested genotypes (IR29 and FL478) with the aim of identifying changes in stoichiometry and subunit composition of complexes in response to salt stress. When the abundances of the identified proteins were compared between salt treated and control plants, a total of 34 proteins were showed more than 1.7-fold change in abundance ($p \leq 0.01$). Eleven proteins were increased and 23 were decreased in abundance in response to salt stress. Of these, several were identified as components of multi-protein complexes. This indicates that subunit stoichiometry of these complexes are changed either as consequence of salt buildup or as part of adaptation mechanisms to salt stress. For example, the abundance of proteins belonging to photosystem II reaction center complex including PsbB, PsbE, and PsbH (Table 2) and chlorophyll a-b binding protein of LHCII type III (spot 69, LHBC) was decreased in the salt-sensitive IR29 during salt stress. Interestingly, PsbB was detected in two separate sub-complexes (complexes f and h) and in both showed a decreased abundance in IR29. Decreased abundance of proteins related to PSII suggested that photosynthetic electron transport might be interrupted in this genotype. Impaired PSII activity may result in loss of net photosynthesis and growth and probably increases PSII-dependent ROS production in the light (Hosseini et al., 2015). However, it should be noted that reduction in growth under salt stress is an adaptive strategy that plants utilize to survive under stress conditions since it allows the plant to rely on multiple resources (Zhu, 2001). In RuBisCo complex, the large subunit showed a decreased abundance (spots 77 and 79) in IR29 and proved to be highly prone to degradation. Decreased abundance of RuBisCo will result in limited photosynthetic carbon fixation and further lead to decreased abundance of enzymes associated with the Calvin cycle. In addition, the abundance of TPI (spot 20) and ENO1 (spot 116), enzymes associated with the glycolytic pathways, was also decreased in IR29. As noted above, TPI was found to interact with ENO1 and this interaction is thought to be part of a larger metabolon that forms to enhance substrate channeling between glycolytic enzymes. In our previous study, the abundance of ENO was also decreased in IR29 (Hosseini et al., 2015), proving its critical role in adaptation to salt stress.

In the salt-tolerant FL478, we found an increased abundance of proteins such as the malic enzyme (NADP-ME2, spot 37), ferredoxin-dependent glutamate synthase (spot 120), fructose-bisphosphate aldolase (spot 87), and ATP synthase subunit beta (spots 91 and 61). NADP-ME2 catalyzes the oxidative decarboxylation of malate to yield pyruvate, CO_2, and NADPH. The resulting NADPH is used as reducing power for other biosynthetic pathways. Increased abundance of ATP synthase beta subunit might be associated with higher ATP production, since it is the catalytic subunit of the ATP synthase complex that generates ATP as an immediate energy source for cells. The abundance of TKT1 (spot 42), identified as dimeric protein, was decreased in FL478. TKT catalyzes the transfer of a 2-carbon ketol residue from a ketose donor to an aldose acceptor in opposing directions in the Calvin cycle and pentose phosphate pathway. TKT is known to play an important role in photosynthesis carbon assimilation since a small suppression of its expression in tobacco using antisense technology led to a dramatic reduction in photosynthesis and phenylpropanoid metabolism (Henkes et al., 2001).

Catalase isozyme A (CATA, spot 38), which was identified as homo-tetrameric protein, was increased in both genotypes, but to a larger extent, in the salt-tolerant FL478 (over 5-fold). CAT is a ROS scavenging enzyme that protects cells from the toxic effects of hydrogen peroxide. Tobacco plants knocked down for CAT exhibited enhanced sensitivity to oxidative stresses under high light and salinity, suggesting an important role for CAT in circumventing stress–induced oxidative stresses (Willekens et al., 1997). Greater up-regulation of CAT in the salt-tolerant FL478 indicated that this genotype performed well in managing oxidative stresses associated with salinity compared to IR29.

4. Conclusion

2D-BN/SDS-PAGE coupled with tandem mass spectrometry for protein identification allowed us to explore the whole cell lysate

complexome of rice. Using this approach, we could identify 30 homo-multimers and 9 hetero-multimers. We were also able to identify novel protein-protein interactions indicating the suitability of the approach in investigation of the complexome of unexplored cellular fractions. In addition, comparative proteomic analysis showed that photosynthesis electron transport and the Calvin cycle-related enzymes were significantly decreased in the salt-sensitive genotype, IR29. This indicates that greater reduction in growth in this genotype might be due to the perturbation of photosynthetic carbon fixation. These results suggested that the salt sensitivity of IR29 is mostly related to its inability to maintain the photosynthetic apparatus in healthy state under salinity and/or its inability to manage oxidative stresses imposed by the excess accumulation of salt.

Author contribution

ASH, JG, and GHS conceived and designed the study and participated in data analysis, ASH performed research, FS, GN, and SAH helped in research, JG wrote the paper. All authors read and approved the final manuscript.

Acknowledgement

This research was funded by a grant provided by the Genetics & Agricultural Biotechnology Institute of Tabarestan, Sari, Iran.

Appendix A. Supplementary data

Supplementary data associated with this article can be found, in the online version, at http://dx.doi.org/10.1016/j.jplph.2016.05.023.

References

Andersson, I., Backlund, A., 2008. Structure and function of Rubisco. Plant Physiol. Biochem. 46, 275–291.
Apse, M.P., Blumwald, E., 2002. Engineering salt tolerance in plants. Curr. Opin. Biotechnol. 13, 146–150.
Bonilla, P., Mackell, D., Deal, K., Gregorio, G., 2002. RFLP and SSLP mapping of salinity tolerance genes in chromosome 1 of rice (Oryza sativa L.) using recombinant inbred lines. Philipp. Agric. Sci. 85, 68–76.
Camacho-Carvajal, M.M., Wollscheid, B., Aebersold, R., Steimle, V., Schamel, W.W.A., 2004. Two-dimensional blue native/SDS gel electrophoresis of multi-protein complexes from whole cellular lysates: a PROTEOMICS APPROACH. Mol. Cell. Proteom. 3, 176–182.
Deinlein, U., Stephan, A.B., Horie, T., Luo, W., Xu, G., Schroeder, J.I., 2014. Plant salt-tolerance mechanisms. Trends Plant Sci. 19, 371–379.
Drewes, G., Bouwmeester, T., 2003. Global approaches to protein-protein interactions. Curr. Opin. Cell Biol. 15, 199–205.
Eubel, H., Braun, H.P., Millar, A.H., 2005. Blue-native PAGE in plants: a tool in analysis of protein-protein interactions. Plant Methods 1, 11.
Götz, S., García-Gómez, J.M., Terol, J., Williams, T.D., Nagaraj, S.H., Nueda, M.J., et al., 2008. High-throughput functional annotation and data mining with the Blast2GO suite. Nucleic Acids Res. 36, 3420–3435.
Gavin, A.-C., Bosche, M., Krause, R., Grandi, P., Marzioch, M., Bauer, A., et al., 2002. Functional organization of the yeast proteome by systematic analysis of protein complexes. Nature 415, 141–147.
Gerhardt, S., Echt, S., Busch, M., Freigang, J., Auerbach, G., Bader, G., et al., 2003. Structure and properties of an engineered transketolase from maize. Plant Physiol. 132, 1941–1949.
Ghaffari, A., Gharechahi, J., Nakhoda, B., Salekdeh, G.H., 2014. Physiology and proteome responses of two contrasting rice mutants and their wild type parent under salt stress conditions at the vegetative stage. J. Plant Physiol. 171, 31–44.
Graham, J.W.A., Williams, T.C.R., Morgan, M., Fernie, A.R., Ratcliffe, R.G., Sweetlove, L.J., 2007. Glycolytic enzymes associate dynamically with mitochondria in response to respiratory demand and support substrate channeling. Plant Cell. 19, 3723–3738.
Grattan, S., Zeng, L., Shannon, M., Roberts, S., 2002. Rice is more sensitive to salinity than previously thought. Calif. Agric. 56, 189–198.
Gregorio, G., Senadhira, D., Mendoza, R., Manigbas, N., Roxas, J., Guerta, C., 2002. Progress in breeding for salinity tolerance and associated abiotic stresses in rice. Field Crops Res. 76, 91–101.
Groth, G., Pohl, E., 2001. The structure of the chloroplast F1-ATPase at 3.2 A resolution. J. Biol. Chem. 276, 1345–1352.
Henkes, S., Sonnewald, U., Badur, R., Flachmann, R., Stitt, M., 2001. A small decrease of plastid transketolase activity in antisense tobacco transformants has dramatic effects on photosynthesis and phenylpropanoid metabolism. Plant Cell. 13, 535–551.
Hosseini, S.A., Gharechahi, J., Heidari, M., Koobaz, P., Abdollahi, S., Mirzaei, M., et al., 2015. Comparative proteomic and physiological characterisation of two closely related rice genotypes with contrasting responses to salt stress. Funct. Plant Biol. 42, 527–542.
Hsieh, J.Y., Chen, S.H., Hung, H.C., 2009. Functional roles of the tetramer organization of malic enzyme. J. Biol. Chem. 284, 18096–18105.
Jensen, L.J., Kuhn, M., Stark, M., Chaffron, S., Creevey, C., Muller, J., et al., 2009. STRING 8—a global view on proteins and their functional interactions in 630 organisms. Nucleic Acids Res. 37, D412–D416.
Kang, D., Gho, S.G., Suh, M., Kang, C., 2002. Highly sensitive and fast protein detection with coomassie brilliant blue in sodium dodecyl sulfate-polyacrylamide gel electrophoresis. Bull. Korean Chem. Soc. 11, 1511–1512.
Lasserre, J.P., Beyne, E., Pyndiah, S., Lapaillerie, D., Claverol, S., Bonneu, M., 2006. A complexomic study of Escherichia coli using two-dimensional blue native/SDS polyacrylamide gel electrophoresis. Electrophoresis 27, 3306–3321.
Linh le, H., Linh, T.H., Xuan, T.D., Ham le, H., Ismail, A.M., Khanh, T.D., 2012. Molecular breeding to improve salt tolerance of rice (Oryza sativa L.) in the red river delta of vietnam. Int. J. Plant Genomics 2012, 949038.
McCarty, R.E., Evron, Y., Johnson, E.A., 2000. The chloroplast ATP synthase: a rotary enzyme. Annu. Rev. Plant Physiol. Plant Mol. Biol. 51, 83–109.
Miteva, Y.V., Budayeva, H.G., Cristea, I.M., 2013. Proteomics-based methods for discovery, quantification, and validation of protein-protein interactions. Anal. Chem. 85, 749–768.
Muller, C.S., Bildl, W., Haupt, A., Ellenrieder, L., Becker, T., Hunte, C., et al., 2015. Cryo-slicing BN-MS – a novel technology for high-resolution complexome profiling. Mol. Cell. Proteom. 15, 669–681.
Munns, R., Tester, M., 2008. Mechanisms of salinity tolerance. Annu. Rev. Plant Biol. 59, 651–681.
Munns, R., 2002. Comparative physiology of salt and water stress. Plant Cell Environ. 25, 239–250.
Munns, R., 2005. Genes and salt tolerance: bringing them together. New Phytol. 167, 645–663.
Negrão, S., Courtois, B., Ahmadi, N., Abreu, I., Saibo, N., Oliveira, M.M., 2011. Recent updates on salinity stress in rice: from physiological to molecular responses. Crit. Rev. Plant Sci. 30, 329–377.
Nelson, N., Yocum, C.F., 2006. Structure and function of photosystems I and II. Annu. Rev. Plant Biol. 57, 521–565.
Ray, M., Mishra, P., Das, P., Sabat, S.C., 2012. Expression and purification of soluble bio-active rice plant catalase-A from recombinant Escherichia coli. J. Biotechnol. 157, 12–19.
Reisinger, V., Eichacker, L.A., 2007. How to analyze protein complexes by 2D blue native SDS-PAGE. Proteomics 7 (Suppl. 1), 6–16.
Remmerie, N., Roef, L., Van De Slijke, E., Van Leene, J., Persiau, G., Eeckhout, D., et al., 2009. A bioanalytical method for the proteome wide display and analysis of protein complexes from whole plant cell lysates. Proteomics 9, 598–609.
Remmerie, N., De Vijlder, T., Valkenborg, D., Laukens, K., Smets, K., Vreeken, J., et al., 2011. Unraveling tobacco BY-2 protein complexes with BN PAGE/LC–MS/MS and clustering methods. J. Proteom. 74, 1201–1217.
Rigaut, G., Shevchenko, A., Rutz, B., Wilm, M., Mann, M., Seraphin, B., 1999. A generic protein purification method for protein complex characterization and proteome exploration. Nat. Biotechnol. 17, 1030–1032.
Schägger, H., von Jagow, G., 1991. Blue native electrophoresis for isolation of membrane protein complexes in enzymatically active form. Anal. Biochem. 199, 223–231.
Schagger, H., Cramer, W.A., Vonjagow, G., 1994. Analysis of molecular masses and oligomeric states of protein complexes by blue native electrophoresis and isolation of membrane protein complexes by two-dimensional native electrophoresis. Anal. Biochem. 217, 220–230.
Schagger, H., 2006. Tricine-SDS-PAGE. Nat. Protoc. 1, 16–22.
Seabra, A.R., Carvalho, H., Pereira, P.J., 2009. Crystallization and preliminary crystallographic characterization of glutamine synthetase from Medicago truncatula. Acta Crystallogr. Sect. F Struct. Biol. Cryst. Commun. 65, 1309–1312.
Shekari, F., Taei, A., Pan, T.L., Wang, P.W., Baharvand, H., Salekdeh, G.H., 2011. Identification of cytoplasmic and membrane-associated complexes in human embryonic stem cells using blue native PAGE. Mol. Biosyst. 7, 2688–2701.
Sherawat, M., Tolan, D.R., Allen, K.N., 2008. Structure of a rabbit muscle fructose-1,6-bisphosphate aldolase A dimer variant. Acta Crystallogr. D Biol. Crystallogr. 64, 543–550.
Shi, Y., Mowery, R.A., Ashley, J., Hentz, M., Ramirez, A.J., Bilgicer, B., et al., 2012. Abnormal SDS-PAGE migration of cytosolic proteins can identify domains and mechanisms that control surfactant binding. Protein Sci. 21, 1197–1209.
Sweetlove, L.J., Fernie, A.R., 2013. The spatial organization of metabolism within the plant cell. Annu. Rev. Plant Biol. 64, 723–746.
Unno, H., Uchida, T., Sugawara, H., Kurisu, G., Sugiyama, T., Yamaya, T., et al., 2006. Atomic structure of plant glutamine synthetase: a key enzyme for plant productivity. J. Biol. Chem. 281, 29287–29296.
Walia, H., Wilson, C., Condamine, P., Liu, X., Ismail, A.M., Zeng, L., et al., 2005. Comparative transcriptional profiling of two contrasting rice genotypes under salinity stress during the vegetative growth stage. Plant Physiol. 139, 822–835.
Wehmeyer, B., Cashmore, A.R., Schäfer, E., 1990. Photocontrol of the expression of genes encoding chlorophyll a/b binding proteins and small subunit of

ribulose-1, 5-bisphosphate carboxylase in etiolated seedlings of Lycopersicon esculentum (L.) and Nicotiana tabacum (L.). Plant Physiol. 93, 990–997.
Willekens, H., Chamnongpol, S., Davey, M., Schraudner, M., Langebartels, C., Van Montagu, M., et al., 1997. Catalase is a sink for H2O2 and is indispensable for stress defence in C3 plants. EMBO J. 16, 4806–4816.
Wittig, I., Braun, H.-P., Schagger, H., 2006. Blue native PAGE. Nat. Protoc. 1, 418–428.
Yoshida, S., Forno, D., Lock, J., Gomez, K., 1976. A Laboratory Manual for the Physiological Studies of Rice. IRRI, Manila, pp. 54.
L. Zeng, M.C. Shannon, 2000. Salinity effects on seedling growth and yield components of rice.
Zhu, J.K., 2001. Plant salt tolerance. Trends Plant Sci. 6, 66–71.